焊接裂纹金属磁记忆信号的特征提取与应用

邸新杰[1], 李午申[1], 严春妍[1], 白世武[1,2], 刘方明[1,2], 薛振奎[2]

(1.天津大学 材料科学与工程学院, 天津 300072;
2.中国石油天然气管道科学研究院, 河北 廊坊 065000)

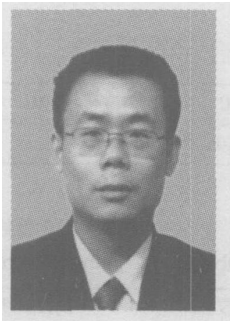

邸新杰

摘 要: 金属磁记忆检测技术是一种新兴的对铁磁性材料进行早期损伤诊断的无损检测方法。通过对焊接裂纹磁记忆信号的小波能量谱特征进行研究表明, 与无裂纹时相比, 含有焊接裂纹信息的金属磁记忆信号, 其尺度-小波能量谱的分布范围广, 能量水平高, 且能量达到峰值以后, 呈指数规律下降, 据此可以判定被测试件中是否含有裂纹缺陷; 其空间-小波能量集中程度较无裂纹时高, 而能量集中的位置恰好就是焊接裂纹存在的位置。

关键词: 金属磁记忆; 焊接裂纹; 尺度-小波能量谱; 空间-小波能量谱

中图分类号: TG115.28 文献标识码: A 文章编号: 0253-360X(2006)02-19-04

0 序 言

金属磁记忆检测是一种基于磁记忆效应的全新的无损检测技术和诊断方法, 与常规的无损检测方法相比, 它的独特之处在于能够对设备和结构进行早期的损伤诊断, 从而防止设备和结构突发性破坏事故的发生。该检测方法一经提出, 就得到了各国无损检测研究者的关注, 他们相继在金属磁记忆的原理和应用方面进行了大量的研究[1]。但迄今为止, 由于没有找到恰当的定量特征, 金属磁记忆检测技术还强烈的依赖于人的经验, 并只能对设备和结构存在的缺陷进行定性的评估, 在找出可能发生损坏的可疑区域后, 还需要采用其它无损检测方法进行确认, 这就限制了金属磁记忆检测方法在工业检测中的应用, 因此对金属磁记忆信号进行定量的分析, 并找出产生缺陷的判据就具有重要的工程实用价值[2]。

裂纹是焊接结构中最为危险的一种缺陷, 它往往导致灾难性事故的发生。由于焊接裂纹产生必然伴随着严重的应力集中, 而这种应力集中状态可以通过对磁记忆信号的分析加以评估。要用磁记忆方法定量的检测焊接裂纹必须正确的提取焊接裂纹磁记忆信号的特征, 这直接关系到裂纹识别结果的准确性。利用金属磁记忆信号的连续小波变换能谱对信号中焊接裂纹信息的特征进行分析。

收稿日期: 2005-05-17

基金项目: 国家自然科学基金资助项目(50475113); 高等学校博士学科点专项基金资助项目(20030056002)

1 连续小波变换的能量谱[3~6]

若能量有限的任意信号函数 $f_1(x)$, $f_2(x)\in R$, $\varphi(x)$满足小波的容许性条件, 则有

$$<f_1, f_2> = C_\varphi^{-1} \iint_{R^2} <f_1, \varphi_{a,b}><\varphi_{a,b}, f_2> \frac{da\,db}{a^2}。 \tag{1}$$

当 $f_1 = f_2 = f$时, 式(1)变为

$$\int_R f(x)|^2 dt = \frac{1}{C_\varphi} \iint_{R^2} |W_\varphi f(a,b)|^2 \frac{da\,db}{a^2}。 \tag{2}$$

由式(2), 若把 $E(a,b) = \frac{|W_\varphi f(a,b)|^2}{C_\varphi a^2}$看作是信号 $f(x)$在(a,b)平面上的能谱密度, 则 $\frac{|W_\varphi f(a,b)|^2}{C_\varphi a^2}\Delta a\Delta b$给出了以尺度 a和空间 b为中心的, 尺度间隔为 Δa、空间间隔为 Δb的能量。

由此, 信号的能量可以表示为

$$E_f = \int_R |f(x)^2|\,dt = \int_R E(b)\,db = \int_R \frac{E(a)}{C_\varphi a^2} da, \tag{3}$$

式中: $E(a) = \int_R |W_\varphi f(a,b)|^2 db$代表小波能量沿尺度轴的分布, 称为信号的尺度—小波能量谱; $E(b) = \int_R \frac{|W_\varphi f(a,b)|^2}{C_\varphi a^2} da$代表小波能量沿空间轴的分布, 称为信号的空间—小波能量谱。

2 金属磁记忆检测试验

2.1 试验材料

试验材料取自“西气东输”工程所用 X70管线钢的板材,这是一种具有较高强度和韧性的针状铁素体管线钢,其主要化学成分及力学性能见表 1及表 2.

表 1 X70管线钢主要合金成分(质量分数,%)

Table 1 Compositions of X70 pipeline steel

C	Si	Mn	P	S	Cr	Mo	Ni	Nb	V	Ti	Cu
0.06	0.19	1.58	0.014	0.002	0.024	0.24	0.176	0.05	0.046	0.019	0.23

表 2 X70管线钢的力学性能

Table 2 Mechanical properties of X70 pipeline steel

屈服强度 R_e MPa	抗拉强度 R_m MPa	伸长率 A(%)
604	669	20.3

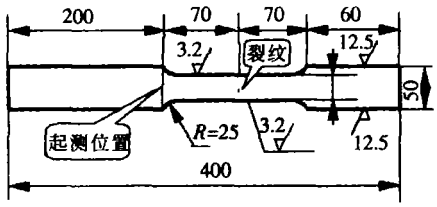

图 1 试件加工图

Fig. 1 Sketch of sample

2.2 试验过程及检测结果

将 X70管线钢制成 400 mm×50 mm×17.5 mm的试件。试件共分两类,加工形式如图 1所示,其中第 1类试件没有预制裂纹,第 2类试件采用线切割的方法加工出一道长度为 3 mm的预制裂纹,并用焊接的方法将预制裂纹埋于试件内部。然后对试件进行退火处理以消除残余应力。退火后在拉伸试验机上进行拉伸试验。在拉伸过程中,分别在试样的弹性变形阶段和产生缩径以后进行磁记忆检测,部分试件的检测结果如图 2所示。第 1类试件在距起测位置 83mm处产生缩径,第 2类试件在预制裂纹处产生缩径。

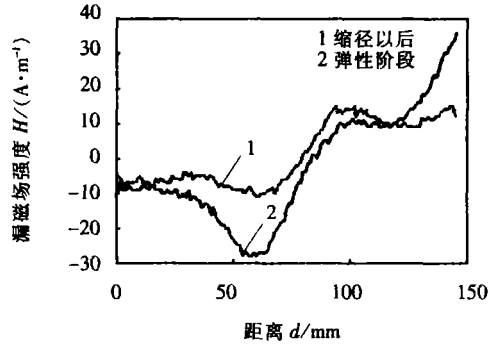

(a) 第 1 类试件检测结果

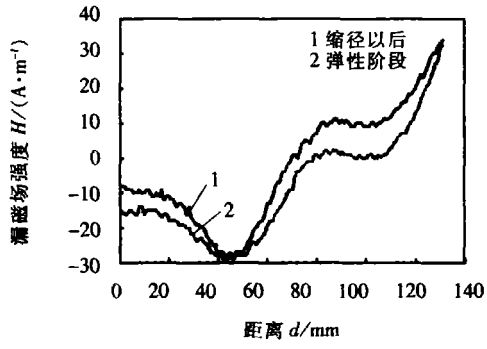

(b) 第 2 类试件检测结果

图 2 拉伸后的磁记忆检测结果

Fig. 2 Metal magnetic memory test result after tension

3 焊接裂纹磁记忆信号的能谱特征分析

金属磁记忆信号反应了被测试件自有漏磁场的法向分量,对于每一条磁记忆曲线,可以把它看作自有漏磁场法向分量 H_p 随检测距离 x的变化,记做 $H_p(x)$。因为 $H_p(x)\in R$,满足式(1)成立的条件,所以磁记忆信号的尺度—小波能量谱和空间—小波能量谱可以表示为式(4)、(5)的形式

$$E(a)=\int_R |W_\varphi H_p(a,b)|^2 \mathrm{d}b. \tag{4}$$

$$E(b)=\int_R \frac{|W_\varphi H_p(a,b)|^2}{C_\varphi a^2}\mathrm{d}a. \tag{5}$$

利用 Morlet小波作为基函数对试验结果进行连续小波变换,然后根据式(4)、(5)计算尺度—小波能量谱和空间—小波能量谱。试件不同阶段磁记忆曲线的尺度 -小波能量谱和空间—小波能量谱如图 3、4所示。

由图 3a可以看出,当取分解尺度范围为

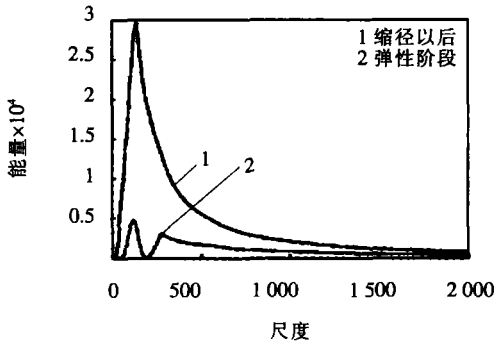

(a)磁记忆曲线的尺度-小波能量谱

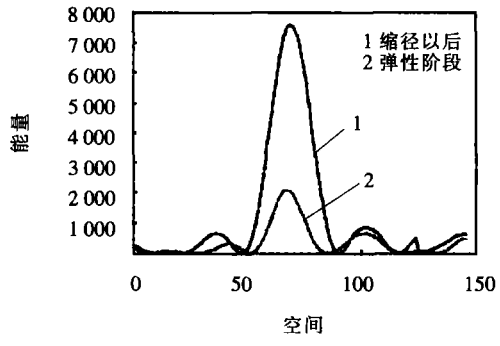

(b)磁记忆曲线的空间-小波能量谱

图 3　第 1类试件磁记忆曲线的小波能量谱

Fig. 3　Metalmagnetic memory wavelet energy spectrum of first sample

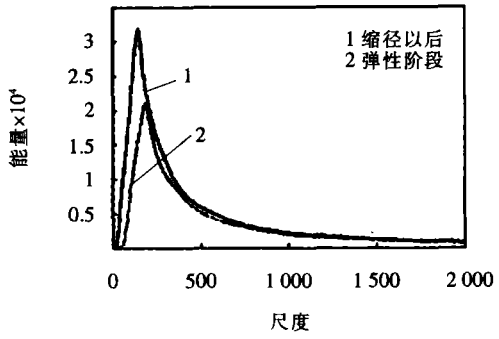

(a)磁记忆曲线的尺度-小波能量谱

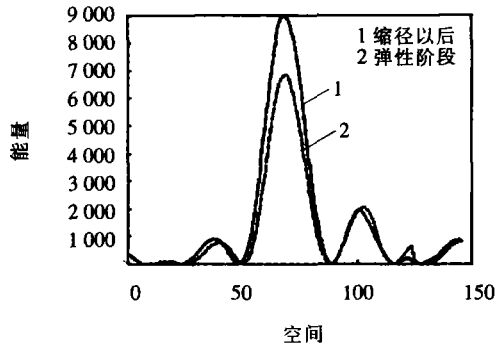

(b)磁记忆曲线的空间-小波能量谱

图 4　第 2类试件磁记忆曲线的小波能量谱

Fig. 4　Metalmagnetic memory wavelet energy spectrum of second sample

[0, 2 000]时,试件在弹性应变阶段和发生缩径以后磁记忆信号的尺度—小波能量谱具有很大的差异,发生缩径以后能量谱的峰值接近弹性阶段能量谱峰值的 6倍,并且达到峰值以后,呈指数规律下降;在图 4a中,试件弹性阶段和发生缩径以后的尺度—小波能量谱相似,并且与图 3a中的缩径后的曲线具有相同的特点,这是由于试件发生缩径时内部产生微裂纹引起应力集中增大造成的,属于裂纹部位漏磁场的一种尺度—小波能量谱线特征,可简称为裂纹的尺度谱线特征。

具有预制裂纹的试件,不论在弹性应变阶段,还是在缩径后,其尺度谱线特征均相同。这是由于预制裂纹的存在,即使在弹性应变阶段,裂纹尖端也会产生严重的应力集中,并导致发生局部塑性变形,当应力达到一定程度时,就会产生微裂纹扩展,所以此时的磁记忆信号具有了裂纹的尺度谱线特征。对于没有预制裂纹的试件,弹性阶段不存在裂纹,没有明显的裂纹尺度谱线特征,但当试件发生缩径产生微裂纹时,才产生明显的裂纹尺度谱线特征。

图 3b, 4b分别表示了试件在不同拉伸阶段的空间—小波能量谱。由图中可以看出,当试件中存在微裂纹时,会在裂纹存在位置产生严重的能量集中,可以称之为空间谱线特征。

4　试验结果的应用

上述分析是基于试验条件下进行的,为了验证上述试验结果,作者对某钢管公司生产现场出现焊接裂纹的钢管利用金属磁记忆检测仪进行了现场检测,并对检测结果进行了小波能谱分析。

钢管的各项工艺参数如表 3所示。被测钢管上的两条焊接裂纹分别位于距起测位置 137 mm 和 241 mm 处的焊接热影响区。为了更好地研究焊接裂纹存在区域金属磁记忆信号的特征,作者分别对有无焊接裂纹存在的焊缝进行了检测,检测结果如图 5所示。

表 3　检测钢管的工艺参数

Table 3　Parameters of pipeline

材料	直径 d /mm	壁厚 δ /mm	状态
X70	1 016	17. 5	焊接后

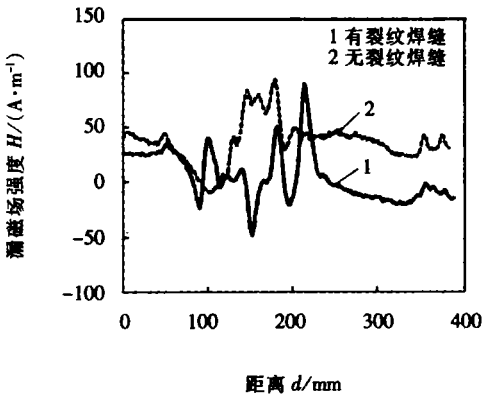

图 5 金属磁记忆检测信号

Fig. 5 Metalmagnetic memory signal

图 6是对上述检测结果进行小波变换后的能量谱。由图 6a中可以看出，有裂纹存在时，尺度 –小波能谱与图 3a中的曲线具有相同的分布形式，能量谱在达到峰值以后，呈指数规律衰减。无裂纹时，能量谱主要分布在一个尺度区间内，当大于这个尺度区间时，能量分布变得平缓，与图 3a的曲线相似。另外无裂纹时的能量水平远远小于存在裂纹时能量水平，与图 3a的规律相符合。这说明试验研究的裂纹尺度谱线可以用于实际裂纹的检测，并可便捷地判断出含有裂纹信息的磁记忆曲线。

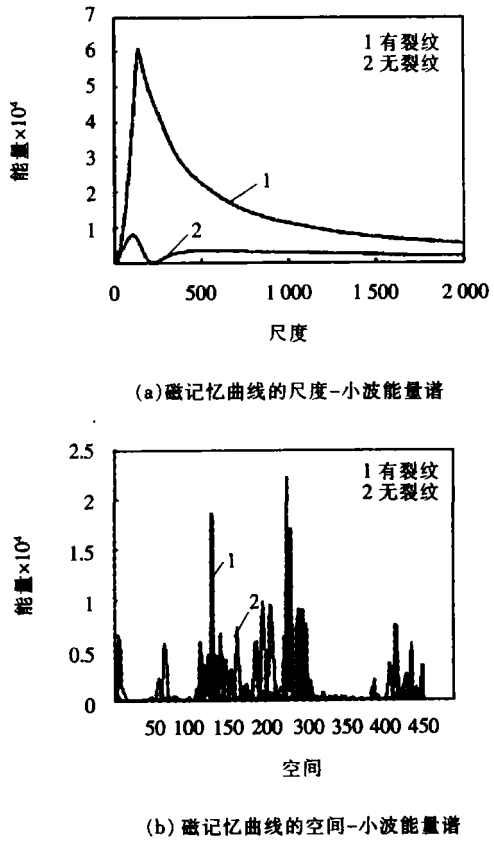

图 6 磁记忆信号的小波能量谱

Fig. 6 Waveletpower spectrum ofmetal magnetic memory signal

图 6b是检测曲线的空间 –小波能量谱，有裂纹存在时，空间 –小波能量谱主要集中在裂纹位置附近，没有裂纹时，空间 –小波能量谱分布分散。这是因为由于焊接过程的影响，在钢管的焊缝区存在着较大应力集中区，造成该区域漏磁场强度增大。

5 结 论

(1) 含有裂纹信息的金属磁记忆信号曲线，其尺度 –小波能量谱的分布范围广，能量水平高，且能量达到峰值以后，呈指数规律下降，据此可以判定被测试件中是否含有裂纹缺陷。

(2) 对于存在裂纹的区域，通过寻找空间 –小波能量谱的能量集中的位置，可以较为准确的确定出裂纹存在的位置。

(3) 研究为金属磁记忆检测方法在实际工程检测中不依赖其它检测方式而独立的完成检测任务提供了基础，具有重要的工程实用价值。

参考文献：

[1] 张卫民，董韶平，张之敬. 金属磁记忆检测技术的现状与发展[J]. 中国机械工程，2003，14(10)：892－896.

[2] 邸新杰. 焊接裂纹金属磁记忆漏磁场的特性研究[D]. 天津：天津大学，2004.

[3] 王蕴红，刘国岁，王一丁. 基于短时傅立叶变换的目标识别方法[J]. 模式识别与人工智能，1998，11(2)：206－210.

[4] 秦前清，杨宗凯. 实用小波分析[M]. 西安：西安电子科技大学出版社，1995：49－56.

[5] WangW J，Mcfadden P D. Application of orthogonalwavelets to early gear damage detection[J]. Mechanical System and Signal Processing，1995，9(5)：497－507.

[6] Jing Lin，Liangsheng Qu. Feature extraction based on morlet wavelet and its application for mechanical fault diagnosis[J]. Journal of Sound and Vibration，2000，234(1)：135－148.

作者简介：邸新杰，男，1973年生，博士研究生。主要从事焊接裂纹金属磁记忆的定量化研究工作，发表论文 3篇。

Email：dixinjie@eyou.com

MAIN TOPICS, ABSTRACTS & KEY WORDS

Numerical simulation and experiment study on keyhole in laser penetration welding WANG Zhi-yong, CHU Xin-jun, CHEN Hong, ZUO Tie-chuan (Laser Insititute, Beijing University of Technology, Beijing 100022, China). p1 – 5

Abstract: Energy balance, pressure balance and temperature of keyhole were analyzed based on the assumption that the keyhole is a Paraboloid of revolution. The keyhole depth and width were calculated by numerical iterative method. The calculated results accord with those of the actual experiments. Then the keyhole principle fitted for low speed laser welding on the assumption that the keyhole with cylinder was developed to a high speed.

Key words: laser deep penetration welding; keyhole; welding pool; revolution paraboloid; mathematical model

Influential factors in laser-MAG hybrid welding process WANG Wei[1], WANG Xu-you[1], ZHAO Zi-liang[2], LENG Kai-bo[2], BU Da-chuan[1] (1. Harbin Welding Institute, Harbin 150080, China; 2. Harbin Jian Cheng Machine Company limited, Harbin 150030, China). p6 – 10

Abstract: Some influential factors in laser-MAG hybrid welding process were analyzed. By the analyzing device of welding arc, it was found that when the distance between laser spot and wire tip is 1mm, the penetration of hybrid welding increase to 1.5 times which compared with conventional MAG welding, and hybrid welding can also improve spreadability, increase weld width, reduce undercut and so on. Hybrid welding as laser welding gets the maximal penetration when laser focus was located 1mm below the top surface of the plate.

Key words: laser-arc hybrid welding; laser welding; arc stability

Experiment on dressing for improving fatigue strengths of welded joints with low transformation temperature electrode FENG Zhao-long, HUO Li-xing, WANG Wen-xian, ZHANG Yu-feng (Material Institute, Tianjin University, Tianjin 300072, China). p11 – 14

Abstract: The fatigue strengths of welded joints in welded structures are much lower than those of the base metal because there are stress concentrations and tensile residual stresses at weld toe. Low transformation temperature electrodes (LTTE) dressing is an useful method for improving the fatigue strengths of welded joint. The fatigue tests of LTTE dressing were carried out on both transverse and longitudinal fillet welded joints. At cycles of 2×10^6, the fatigue strengths of LTTE dressing are 154.7 MPa and 173.9 MPa, respectively, which is 101.4% and 100.3% of those of TIG dressing. This shows that LTTE dressing in improving fatigue strength is useful or better than TIG dressing, while LTTE dressing is easier than TIG dressing and it can deal with different position of weld beams.

Key words: TIG dressing; low transformation temperature electrode dressing; welded joints; fatigue strength

Determination of characteristic parameters of weld penetration in electron beam welding of aluminum alloy WU Qing-sheng, FENG Ji-cai, HE Jing-shan (State Key Laboratory of Advanced Welding Production Technology, Harbin Institute of Technology, Harbin 150001, China). p15 – 18

Abstract: Based on the visual image sensing method, extraction of the characteristic parameters of the weld penetration in electron beam welding of aluminum alloy was investigated with the flat plate and the slope plate experiments. The results show that the width of the feature zone (W) responds to the transition of the penetration status from the partial penetration to the full penetration during electron beam welding of aluminum alloy, but the rear part of the length of the feature zone (RL) does not. So the width of the feature zone can be used as the characteristic parameter of the penetration to monitor and control the variation of the penetration status, which provides an effective way for penetration control in electron beam welding of aluminum alloy.

Key words: electron beam welding; penetration; characteristic parameter; aluminum alloy; visual image sensing

Feature extraction of metal magnetic memory signal and its application for weld crack DI Xin-jie[1], LI Wu-shen[1], YAN Chun-yan[1], BAI Shi-wu[1,2], LIU Fang-ming[1,2], XUE Zhen-kui[2] (1. Tianjin University, Tianjin 300072, China; 2. Pipeline Research Institute of China Petroleum Hebei, Lang Fang 065000, China). p19 – 22

Abstract: Metal magnetic memory (MMM) is a new non-destructive testing method which can make a diagnosis for the ferromagnetic material in early damaging stage. The wavelet energy spectrum feature of MMM signal for weld cracks. Research shows that, for MMM signals with cracks, the distribution scope of scale wavelet energy spectrum is wide with a high energy level, and the energy spectrum assumes an exponential attenuation after it reaches a peak, which can be used to estimate whether the sample included crack or not. The space wavelet energy with crack is higher than that without crack. Where the space wavelet energy spectrum

indicates a concentration is the very position of the crack.

Keywords: metal magnetic memory; weld crack; scale wavelet energy spectrum; space wavelet energy spectrum

Pose of ultrasonic phased array scanner in inspecting tuhbular joint welds HAO Guang-ping, DENG Zong-quan (School of Mechanical and Electrical Engineering, Harbin Institute of Technology, Harbin 150001, China). p23-26, 30

Abstract: At present, offshore platforms are welded with steel material. The main weld seams are tubular joint welds and have very complicated shape, which are difficult to realize automatic testing for defect in contrast with the girth welds, longitudinal welds and twist weld seams. An ultrasonic phased array probe scanner with three degrees of freedom was designed and made based on the specialities of tubular joint welds on offshore platform. The pose relation between the scanner and tubular joint weld was set up, the concrete expression methods of pose matrix between phased array probe and weld seam and scanner base were given. The pose matrix method provided automatic control foundation to scanner. The automatic testing to complicated shape welds of tubular joint could be realized by the scanner. The experiments on reference block with the scanner were carried out and the results indicates that the artificial defect on the reference block can be truely inspection. It can satisfy the requirement of automatic testing to tubular joint welds.

Keywords: scanner; phased array probe; tubular joint weld; pose matrix

Laser deposited welding of functional gradient materials with powder feeding SONG Jian-li[1,2], GE Zhi-jun[1], DENG Qi-lin[1], HU De-jin[1] (1. School of Mechanical and Power Engineering, Shanghai Jiaotong University, Shanghai 200030, China; 2. School of Materials Science and Engineering, Taiyuan University of Science & Technology, Taiyuan 030024, China). p27-30

Abstract: Laser deposited welding of stainless steel and iron-based alloy was carried out with synchronized powder feeding method. The microstructure, properties and composition of the deposited layer were thoroughly analyzed and tested by means of microstructural observation, SEM scanning, tensile strength testing, wearing and EDAX analysis. Different process and property requirements at different deposited position can be satisfied with functionally gradient combination of different welding materials. The deposited welding layer presents a metallurgical bonding with the substrate, and the dilution is quite small. The microstructure obtained is fine, compact and free of cracking and porosity. The tensile strength of the samples at the bottom of the deposited layers reaches 752.4MPa, and the elongation 41.05%. The wearing resistance of the surface layer has greatly surpassed that of the substrate. The optimized matching of materials and properties can be realized by laser deposited welding with powder feeding, which provides an effective way for the forming and functional gradient repairing of metal components.

Keywords: laser deposited welding; functional gradient; microstructure and properties; repairing

Numerical analysis of the transport properties for no equilibrium plasma FAN Ding[1], HUANG Yong[1], ZHANG Rui-hua[1], FAN Qing-hua[1], Masao Ushio[2] (1. State Key Laboratory of New Non-ferrous Metal Materials, Lanzhou University of Technology, Lanzhou 730050, China; 2. Joining and Welding Research Institute, Osaka University, Osaka 567, Japan). p31-34

Abstract: Transport properties of non-equilibrium argon plasma were analyzed by using Chapman-Enskog method at low and high pressure and for various temperature difference between electrons and heavy species. Electorns and heavy species were trenled as two different gases and a generalized Suha equation was used to calealate the plasma composition. The results show that the transport properties of no equilibrium plasma are far different from that of local temperuture equilibrium (LTE) plasma. It will result in greater error if the transport properties for LTE plasma are applied to to no-equilibrium plasma.

Keywords: no-equilibrium plasma; transport properties; numerical analysis; two-temperature gases; collision integral

Effect of applied magnetic field on the wear resistance property of Co-based overlay welding alloy LIU Zheng-jun, LIU Duo, CHENG Jiang-bo, SU Yun-hai (School of Material Engineering, Shenyang University of Technology, Shenyang 110023, China). p35-38

Abstract: The effect of applied longitudinal magnetic field on Co-based plasma arc surfacing on low carbon steel was studied. It is found that only the magnetic intensity and weld criterion parameters must be matched properly, the optimal effect of grain refining can be gained. And the discussed emphasis is the influence of magnetic density and welding current on the regularity of hardness and wear resistance of the overlay welding metal. The result indicated that proper electromagnetic field can refine the structure of overlay weld metal but also improve the hardness and wear resistance of the overlay welded mental, which increase the comprehensive mechanical properties of overlay welded metal.

Keywords: longitudinal magnetic field; electromagnetic stirring; Co-based alloy

In situ formation TiC particles reinforced Fe-based alloy composite coating by GTAW SONG Si-li, WANG Xin-hong, ZOU Zeng-da